Chemical Engineering Science 265 (2023) 118197

Contents lists available at ScienceDirect

Chemical Engineering Science

journal homepage: www.elsevier.com/locate/ces

Flow patterns of ionic liquid based aqueous biphasic systems in small channels

Yiota-Victoria Phakoukaki [a], Paul O'Shaughnessy [b], Panagiota Angeli [a,*]

[a] ThAMeS Multiphase, Department of Chemical Engineering, UCL, Torrington Place, London WC1E 7JE, UK
[b] Johnson Matthey Blounts Ct Rd, Sonning Common, Reading RG4 9NH, UK

HIGHLIGHTS

- The flow of ionic liquid based aqueous biphasic systems was studied in small channel systems for the first time.
- Physical properties of three different IL-ABS weight concentration solutions were acquired, including viscosity, density, surface and interfacial tension.
- Flow pattern maps were developed for different ABS solute weight concentrations (18, 20 and 22 wt%) and channel internal diameters (0.2, 0.5 and 0.8 mm).
- Capillary and Reynolds numbers were used to plot a generalized flow pattern map, where the transition boundaries of plug flow collapsed for all experimental conditions.

ARTICLE INFO

Article history:
Received 23 May 2022
Received in revised form 3 October 2022
Accepted 6 October 2022
Available online 13 October 2022

Keywords:
Two-phase flows
Flow patterns
Small channels
Ionic liquids
Aqueous biphasic systems
Process intensification

ABSTRACT

Ionic liquid based aqueous biphasic systems (IL-ABS) were formed by the addition in water of a hydrophilic ionic liquid (1-Butyl-3-methylimidazolium Chloride, C_4mimCl) and a kosmotropic salt (tripotassium phosphate, K_3PO_4). The flow patterns of IL-ABS were studied in capillary channels with 0.2, 0.5 and 0.8 mm internal diameter; this is the first time such two-phase flows have been investigated. Three weight concentrations of the ionic liquid and the salt (18, 20 and 22 wt%) were chosen within the biphasic region. The main flow patterns included plug, dispersed and parallel flow. It was found that both channel diameter and weight concentrations would affect the flow patterns observed. Finally, a generalized flow pattern map was plotted using a combination of capillary and Reynolds numbers, where the transition boundaries of plug flow collapsed for all ionic liquid and salt concentrations studied.

1. Introduction

Since their discovery in the 1890s, aqueous biphasic systems (ABS) have been used for a range of separations including those of various biomolecules and precious metals (Iqbal et al., 2016; Ventura et al., 2017; Smirnova et al., 2021). ABS are defined as water-rich mixtures formed by the addition of two water-soluble compounds that induce the separation of the mixture into two phases. They are ternary systems usually composed of either two polymers (commonly polyethylene glycol, PEG, and Dextran), a polymer and a kosmotropic salt or two salts (one kosmotropic and one chaotropic) (Freire, 2016). In polymer–polymer systems, large aggregates form while steric exclusion encourages the formation of the two immiscible phases. Similarly, in polymer - salt solutions the kosmotropic salt absorbs large amounts of water and the same phenomenon is observed (Iqbal et al., 2016). ABS used in separations have demonstrated high recovery yields and selectivity, while they are environmentally friendly, as they consist mainly of water, economic, and biologically compatible (Wu et al., 2008; Albertsson, 1995). Therefore, they are important for the transition to sustainable bioprocessing.

The majority of separations with conventional polymer-based ABS have mainly been carried out in batch vessels with limited reports of continuous operations. In traditional continuous equipment such as pulsed columns and mixer-settlers, ABS suffered major drawbacks including flooding, back mixing, emulsification, and poor phase separation that drastically limited their operation (Espitia-Saloma et al., 2014). It is therefore imperative to develop novel materials design and engineering approaches that overcome the above drawbacks, to allow the sustainability benefits of ABS to be realised.

* Corresponding author.
E-mail address: p.angeli@ucl.ac.uk (P. Angeli).

https://doi.org/10.1016/j.ces.2022.118197
0009-2509/

Nomenclature

Bo	Bond number = $\frac{D^2\Delta\rho g}{\gamma}$ [-]
Ca	Capillary number = $\frac{\mu_i U_i}{\gamma}$ [-]
D	Internal diameter of channel [m]
g	Gravitational acceleration [m/s]
L	Characteristic length [m]
Q	Volumetric flow rate of fluid [m^3/s]
Re	Reynold number = $\frac{\rho_i U_i D}{\mu_i}$[-]
u	Mixture velocity [m/s]
V	Volume [m^3]
w	Width [m]
We	Weber number = $\frac{\rho_i U_i^2 D}{\gamma}$ [-]
X	Salt phase weight percentage [%]
Y	Ionic liquid weight percentage [%]

Greek symbols

γ	Interfacial tension [N/m]
σ	Surface tension [N/m]
μ	Dynamic viscosity [kg $m^{-1}s^{-1}$]
ρ	Density [kg m^{-3}]
ε	Volume fraction = Q_{IL}/Q_t *[s]*

Subscripts

ABS	Aqueous Biphasic System
B	Bottom phase
c	Continuous phase
d	Dispersed phase
F	Feed concentrations
IL	Ionic liquid
t	Total
T	Top phase
TL	Tie Line
TLL	Tie line length

Recently, a new class of ABS based on ionic liquids (ILs) has been proposed, formed with hydrophilic ILs (chaotropic salts) and kosmotropic salts (Berthod et al., 2008). Ionic liquids are organic salts with melting points below 100 °C. They have unique properties including low vapour pressures, good thermal stability, high ion density and conductivity (Singh and Savoy, 2020). Moreover, when used inABS, IL can significantly affect the equilibrium behaviour. Modifications of both the cation and the anion of the IL enable them to be tailored to meet specific separation requirements. In addition, IL-ABS have lower molecular weight and viscosity than polymer-based ABS which enables faster settling, making them industrially attractive (McQueen and Lai, 2019). The phase separation can be controlled by the different nature of the IL and the salt phase hydrogen bonding properties. Due to their novelty, most of the IL-ABS literature has so far concentrated on the determination and characterization of their phase diagrams and tie lines. A few recent studies have explored their application to the extraction of a range of biomolecules revealing high partition coefficients (Ventura et al., 2017; Louros et al., 2010; Neves et al., 2009; Ventura et al., 2009).

IL-based ABS overcome some of the drawbacks of the conventional ABS systems such as interface precipitation and slow separation resulting to long settling times. Furthermore, the use of small-scale devices can overcome the drawbacks of ABS operation in continuous conventional equipment (Teixeira et al., 2018). Over the past two decades liquid–liquid flows in small channels have been applied to separations, chemical analysis and synthesis (Assmann et al., 2013; Xu and Xie, 2017). The studies revealed that small channels offer several advantages including, selectivity, high mass transfer rates due to increased interfacial area and short residence times, while they are inherently safe due to small equipment size (Wang and Luo, 2017; Seemann et al., 2012; Xu and Xie, 2017; Zhao and Middelberg, 2011; Ciceri et al., 2014). Several studies have considered the hydrodynamics and flow patterns of two-phase liquid flows in micro/small channels, using oil or organic solvents and aqueous solutions as the two phases. (Jovanović et al., 2011; Kashid and Agar, 2007; Tsaoulidis et al., 2013). Moreover, a large number of flow pattern maps have been published focusing on different parameters such as phase velocities (Cao et al., 2018), flow rates (Darekar et al., 2017) or dimensionless numbers such as capillary (Ca), Weber (We) and Reynolds (Re) (Phakoukaki et al., 2022) as coordinates. Nonetheless, the different flow pattern transitions are still difficult to predict and highly dependent on the geometry and physical properties of the systems practiced. Compared to conventional organic-aqueous two-phase systems, which have been extensively studied in the literature, the IL-ABS systems have significantly different physical properties which are expected to affect the flow patterns forming and their boundaries. The most studied flow pattern in liquid–liquid systems is plug/slug flow as it appears over the largest range of experimental parameters (Seemann et al., 2012; Kashid and Agar, 2007; Dore et al., 2012). Plug flow allows for large interfacial areas, improved radial mixing due to circulation patterns found in both phases and reduced axial mixing, which improves uniformity and intensifies mass transfer (Sattari-Najafabadi et al., 2018).

Contrarily, there are limited studies of ABS two-phase flows in small channels. In most of the studies reported in the literature, parallel flow was observed for polymer-based ABS (Frampton et al., 2011; Meagher et al., 2008; Silva et al., 2012). Moreover, previous studies primarily used conventional ABS systems composed of PEG and Dextran, for biomolecule cell enrichment (Soohoo and Walker, 2009; Fang et al., 2012; Tsukamoto et al., 2009). Only limited studies have reported dispersed droplet patterns in microchannels, possibly due to the very low interfacial tension of ABS. Mastiani et al. (2017), had one of the first successful examples of drop formation in microchannels by the addition of high concentrations of PEG and salt and found a broad droplet size distribution. In other cases, to achieve droplet formation, external forces were applied. Ziemecka et al. (2011), actuated droplet formation by perturbing the inlet of the microfluidic device with a piezo-electric bending disc. Similarly, Sauret et al. (2012) introduced a harmonic perturbation to the dispersed phase that led to the formation of droplets and were able to control the fluidic regime by tuning the flow rates, frequency, and amplitude of the external force.

In this work, the flow patterns that form in small channels using IL-based ABS are investigated. To the authors' knowledge, this is the first time that two-phase liquid flows of IL-ABS are studied. The physiochemical interactions of the IL-ABS components determine not only the volume fractions of the two immiscible phases that form in the biphasic region but also their physical properties. The phase diagram of the IL-ABS system was constructed, and the physical properties, such as density, viscosity and interfacial tension of the IL-ABS phases were measured for different initial concentrations of the ionic liquid and the salt. In contrast to common flow pattern maps developed for organic-aqueous phases, the two aqueous based phases of the ABS have larger density differences and viscosities while the interfacial tension is very low

resulting in novel flow observations. The flow patterns were observed in small channels with different internal diameters and with IL-ABS systems of different weight compositions. New transition lines were proposed for the boundaries of plug flow.

2. Experimental set up and procedure

The ionic liquid, 1-Butyl-3-methylimidazolium Chloride, [C_4mim][Cl] at 98 % HPLC grade was purchased from Sigma-Aldrich (UK). The salt tripotassium phosphate (K_3PO_4) at 98 % reagent grade was purchased from Sigma-Aldrich (UK). Fig. 1 illustrates the chemical structures of the ionic liquid and salt ions used for the formation of the aqueous biphasic system. All experiments were carried out at room temperature and pressure (T = 25 ℃).

A phase diagram was determined at 25 ℃ (±1 ℃) by using the cloud point titration method. An aqueous solution of the K_3PO_4 salt was prepared by dissolving a known concentration of the salt (40 wt%) in distilled water. Similarly, aqueous solutions of the hydrophilic ionic liquid were prepared at 80 wt% and added drop by drop to the aqueous inorganic salt solution until first a cloudy and then a biphasic solution was detected. Further details on the experimental procedure followed and tie lines can be found elsewhere (Neves et al., 2009; Ventura et al., 2009; Louros et al., 2010). The weights of the salt, ionic liquid and water at which the biphasic solution was detected, were then used for the determination of the phase diagram boundary line. The phase diagram obtained was in close agreement with literature data, validating the procedure used (Neves et al., 2009; Ventura et al., 2009; Louros et al., 2010).

Once the phase diagram was established, three points within the biphasic region were selected. The three biphasic solutions were prepared and left to equilibrate for 1 min. They were then separated, and their physical properties were measured. Viscosities were measured with a digital Rheometer DV-111 Ultra (Brookfield), while the interfacial, surface tensions and contact angles were measured with the pendant drop method using a DSA30E drop shape analyser (KRÜSS Scientific). The densities of the phases were measured before and after equilibration with a DMA 4500 M density meter (Anton Paar) at a range of temperatures (20–40 ℃).

The continuous biphasic flow studies were carried out in small channels with capillaries of 0.2, 0.5 and 0.8 mm internal diameter. The two ABS phases were fed separately in the main circular test channel via a PTFE *T*-junction inlet configuration using high precision continuous syringe pumps (K_d Scientific). All sub-channels connected to the main capillary had the same internal diameters. The hydrophilic ionic liquid ABS was introduced in the channel at the same axis as the main one, while the salt ABS was fed from the side channel perpendicular to the main one and acted as the dispersed (see Fig. 2). The ionic liquid volume fraction (ε_{IL}) was equal to:

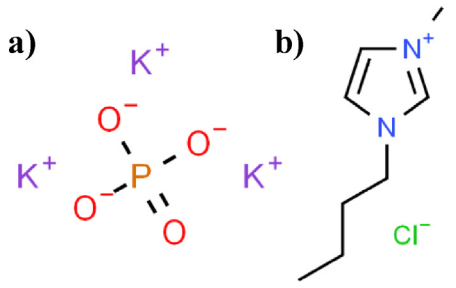

Fig. 1. Chemical structures of the (a) salt and (b) the ionic liquid phase used for the formation of the ionic liquid aqueous biphasic systems.

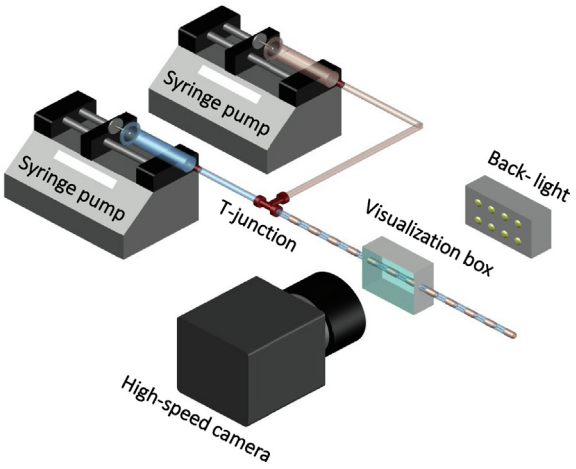

Fig. 2. Experimental set up for the imaging of the two-phase flow patterns in small channels.

$$\varepsilon_{IL} = \frac{Q_{IL}}{Q_{IL} + Q_{Salt}} \quad (1)$$

where Q is the volumetric flow rate of the ionic liquid (IL) and the salt phase (salt).

The flow experiments were performed for three ABS feed weight concentrations; in all cases the salt and the ionic liquid were added at the same weight fraction (18, 20 and 22 wt%). Below these will be referred to as 18, 20 and 22 wt% feed solutions. The flow patterns were visualised and recorded using a ultima high speed camera (Photron Fatcam) at 2000–5000 Hz, depending on the flowrate. The channel section to be visualised was illuminated with a 60 W continuous arc lamp. An enclosing visualization box filled with a water/glycerol mixture to match the refractive index of the materials was used to minimise reflections and improve images.

3. Formation of ABS

The ABS selected is a ternary system composed of water and two solutes, an ionic liquid and a salt. An example of the appearance of the ABS formed by adding C_4mimCl and K_3PO_4 in water is shown in Fig. 3 with an upper IL-rich phase and a lower inorganic-salt rich phase.

Fig. 4 shows an orthogonal representation of the phase diagram with the binodal curve separating the monophasic and biphasic

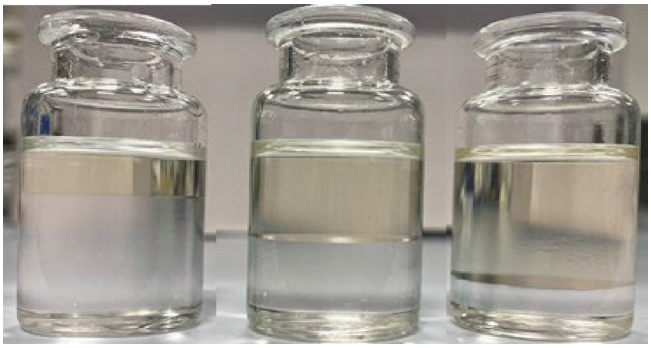

Fig. 3. Ionic liquid aqueous biphasic systems at different points on the tie line; the top is the ionic liquid (C_4mimCl)-rich phase and the bottom is the salt (K_3PO_4)-rich phase.

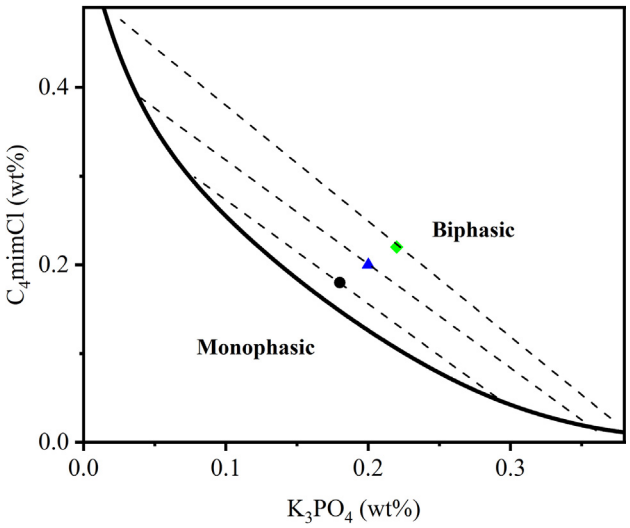

Fig. 4. Phase diagram for ionic liquid/salt/water system: (—) Binodal curve; (---) Tie lines; (●) K_3PO_4 18 wt%, C_4mimCl 18 wt%; (▲) K_3PO_4 20 wt%, C_4mimCl 20 wt%; (♦) K_3PO_4 22 wt%, C_4mimCl 22 wt%.

regions, which was obtained as discussed above. The wt% of water is the difference required to reach 100 % mass in a given mixture composition. For salt and ionic liquid compositions above the binodal curve, a two-phase system of two immiscible phases forms, while at compositions below the curve a monophasic solution is obtained. The binodal curve was validated against Eq. (2) from the literature (Neves et al., 2009).

$$Y = 72.64\exp[-0.319X^{0.5} - 4.07 * 10^{-5}X^{3}] \quad (2)$$

where the IL and salt wt% are Y and X, respectively.

After the determination of the phase diagram, three different weight concentrations of ionic liquid and salt in the biphasic region were prepared, as shown in Fig. 4. The points were selected for the determination of the tie lines (TL) and the tie line lengths (TLL). By increasing the ionic liquid and salt wt% equally by 2 % the three feed points would systematically move away from the binodal curve further into the biphasic region, resulting in longer TLL. The TLL is correlated to the rate at which the two phases separate. In particular, the longer the tie line, the quicker the phases would separate. With mixture volumes of 20 ml, the 18 wt% mixture seperated completely after ~ 45 s while the 22 wt% separated in just 30 s (±4s).

The tie lines are described by Eq. (3) where the constants *a* and *b* are summarised in Table 1. The gradients of the shorter TLL were similar, but that of the longer one, which is also further away from the binodal curve, deviates. This agreed well with the values reported in the literature (Ventura et al., 2011).

$$C_4mimCl(wt\%) = aK_3PO_4(wt\%) + b(wt\%) \quad (3)$$

Table 1
Constants in Eq. (3) for tie lines and calculated Tie Line Length for three different ABS feed compositions.

wt fraction feed composition (%)		a	b	TLL
C_4mim Cl	K_3PO_4			
0.18	0.18	−1.170	39.1	34.83
0.20	0.20	−1.171	43.5	48.51
0.22	0.22	−1.304	51.0	59.61

From the tie lines the actual compositions of the top (T) and bottom (B) phases and the overall system compositions were determined by the lever-arm rule as illustrated in Fig. 5. Furthermore, using the top and bottom phase compositions, the TLL was determined using Eq. (4) (Freire, 2016).

$$TLL = \sqrt{(X_T - X_B)^2 + (Y_T - Y_B)^2} \quad (4)$$

Typically, ABS formation is triggered by the water-solvation competition between the IL ions and salt ions. The salt ions win due to their larger hydration energy in comparison to the IL ions. Subsequently, there is a net flux of water molecules from the hydrophilic IL-rich phase towards the salt-rich phase (Quental et al., 2015). This is confirmed by Fig. 5, where in all three cases, the bottom salt phase always contains a higher percentage of water than the top, ionic liquid-rich phase. With increasing salt concentration, the difference of water weight percentage (wt %) between the top and bottom phases also increases.

This trend is explained by the well-known Hofmeister series, which is a classification of ions based on their salting-in/out ability. This series was originally derived from the observed ordering of different salts based on the minimum concentration needed for protein precipitation to occur from an aqueous solution. This empirically derived series classifies ions as either kosmotropic (order making) or chaotropic (chaos making) depending on their abilities to interact with water and to alter the local instantaneous interactions between water molecules, with anions generally showing much larger 'salting out' effects than cations. A section of the anion Hofmeister series from the most to the least kosmotropic has been reported as (Yang, 2009):

$$F^- \sim SO_4^{2-} > HPO_4^{2-} > C_2H_3O_2^- > Cl^- > Br^- > NO_3^- > ClO_3^- > I^- > ClO_4^- > SCN^-$$

Anions from the beginning of this series through to approximately Cl^- are kosmotropes and will salt-out, while anions near the end of this series are chaotropes and will salt-in (Görgényi et al., 2006). These salting out/in effects are also related to a solute's structure with the magnitude of specific ion effects influenced by molecular attributes of the solute such as: (1) polarizability, (2) molecular size/volume and (3) polarity. The electrostatic interactions between kosmotropic ions and water molecules are more intense than the intermolecular hydrogen bonds. This results in the breaking of hydrogen bonds and the formation of solvated

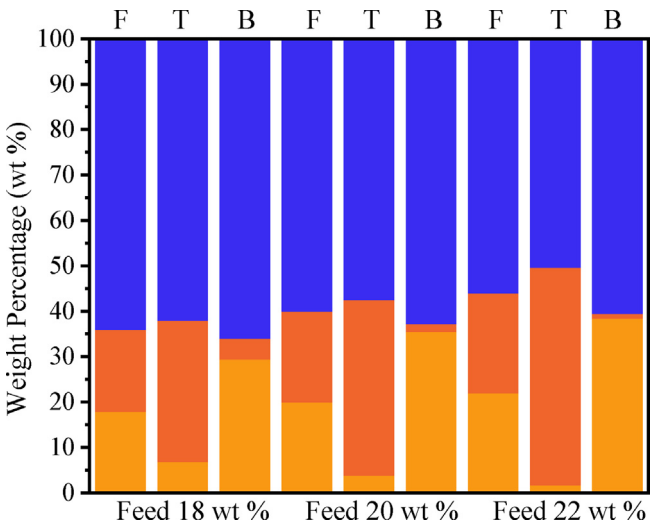

Fig. 5. Compositions of the ABS for the Feed (F), Top (T) and Bottom (B) phases: (■) H_2O wt %; (■) C_4mimCl wt %;(■) K_3PO_4 wt %.

ion structures with a higher degree of order compared to the salt free phase (Long and McDevit, 1952; Wang, Lei, and Wania, 2016). As anions have a greater effect than cations, they will be the only ones considered here. The salt anion (PO_4^{3-}) is more kosmotropic than the ionic liquid anion (Cl^-) on the Hofmeister series, confirming the migration of water to the salt rich phase.

4. ABS physical properties

The properties of the ABS phases, for the same three feed salt and IL concentrations (18, 20 and 22 wt%) shown in Fig. 4, were measured. Density data for all the studied systems are presented in Fig. 6. In general, the density slightly decreases with the increase in temperature, while the density of the salt-rich phase is always significantly higher than that of the IL-rich phase.

In addition, by increasing the concentration of both solutes by equal amount, the density of the salt-rich phase increases from 1.34 to 1.45 g/ml while that of the ionic liquid-rich phase slightly decreases from 1.09 to 1.07 g/ml. This is because the apparent density of the bottom, salt-rich, phase is larger than the apparent density of the top, ionic liquid-rich, phase. Apparent density is defined as the density of the liquid phase, after the contribution of the mass and volume associated to the salt ions has been removed (Dougherty, 2001). Since the inorganic salt is more kosmotropic than the ionic liquid, the salt-rich phase has a higher degree of order than the ionic liquid-rich phase allowing for its molecules to be more closely packed compared to the molecules in the ionic liquid phase. Consequently, not only the density of the salt phase increases, but also the density difference between the two phases increases, which favours phase separation. Compared to traditional polymer-salt ABS, the density differences between the two phases are larger in the IL-ABS and therefore favour phase separation more (Quental et al., 2015).

Table 2 reports the viscosities, surface and interfacial tensions of the IL-rich and the salt-rich phases at 20 °C. Overall, with increasing solute concentrations the viscosities increase, due to the stronger intermolecular forces. In all cases, the viscosity of the salt rich phase is almost double that of the IL phase. The surface tension of both phases is in all cases less than that of water (72 mN/m). The salt-rich phase surface tension is always higher than that of the IL-rich phase due to the higher water content of the salt-rich phase for equal concentrations of IL and salt (See Fig. 5). Overall, the results are in agreement with Weissenborn et al. (1996), who reported that on average the surface tension decreases with increasing salt ion concentration. The major reduction in surface tension occurs until the surface is saturated, and an almost constant surface tension has been reported at high salt concentrations (Ghasemian et al., 2010). Since the overall water content of the salt rich phase remains almost constant, so does the surface tension with a minor decrease from 56 mN/m to 54 mN/m after the initial decrease from the value of water of 72 mN/m. Similarly, the surface tension of the ionic liquid rich phase slightly increases from 48 mN/m to 52 mN/m.

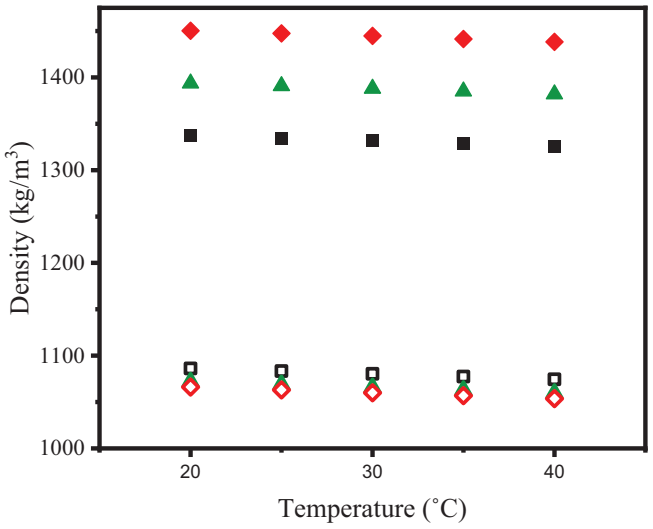

Fig. 6. Density of the aqueous ionic liquid and salt-rich phases with increasing temperature: filled symbols are for the salt-rich phase and open symbols are for the ionic liquid-rich phase (♦) (◊) K_3PO_4, C_4mimCl 22 wt% Feed (▲) (△) K_3PO_4, C_4mimCl 20 wt% Feed; (■) (□) K_3PO_4, C_4mimCl 18 wt% Feed.

The interfacial tension will affect the formation of drops in the small channels and consequently the interfacial area that will be available for mass transfer. By increasing the weight concentration of the two solutes by 2 wt%, the interfacial tension increases significantly. This phenomenon agrees well with literature findings suggesting that the interfacial tension is proportional to the TLL (Bamberger et al., 1985). As the TLL increases and the feed point moves away from the binodal curve so does the interfacial tension, decreasing the required separation time.

5. ABS flow patterns in small channels

During the flow of immiscible liquids in small channels different patterns can form depending on phase flow rates, ratio and inlet geometry, as well as physical properties including density, viscosity, and channel wall wettability (Zhao and Middelberg, 2011). The flow patterns obtained for all three ABS feed solutions in channels with three different internal diameters (0.2, 0.5 and 0.8 mm) are discussed here. The dimensionless numbers relevant to these two-phase flows are Reynolds, capillary, Weber, and Bond number.

According to the literature, for Bond numbers below 0.88 to $(2\pi)^2$ gravitational forces can be considered negligible (Angeli and Gavriilidis, 2008). The Bond numbers calculated for the different channel diameters and ABS weight fractions are given in Table 3. For the 0.2 mm channel, Bo indicates that gravitational forces can be considered negligible for all three ABS feed concentrations. This was confirmed experimentally when the drops in the dispersed pattern were primarily symmetric. For the 0.5 mm channel, however, and at low inlet weight fraction, the Bond number is 2.27, indicating that the gravitational forces cannot be completely neglected. This is due to the low interfacial tension in the ABS 18 wt% system and the larger density difference between the two phases compared to organic-aqueous systems. Finally, for the 0.8 mm channel the Bond numbers, all concentrations are above 1 and mostly higher than the ones reported in the literature for small channels (Phakoukaki et al., 2022), therefore gravity effects cannot be neglected.

The main patterns observed in the small channels are parallel/stratified flow, plug/slug flow, and dispersed flow, as shown in Fig. 7. Other in between flow patterns were also observed that will be discussed under one of these three main categories. In the *T*-Junction inlet configuration, the phase that is fed along the main axis of the flow can be either continuous or dispersed. This depends on the coating or material of the channel and the viscosity of the liquids; highly viscous fluids tend to be in contact with the channel wall (Qian et al., 2019). It has also been shown that the channel inlet geometry can have a significant effect on the flow patterns in small channels (Tsaoulidis et al., 2013).

The two phases of the ABS are predominantly water based. Their contact angles were measured on Teflon planar surfaces, of the same material as the small channel walls. Since Teflon is hydrophobic, both phases have contact angles >90°. The ionic liquid

Table 2
Physical properties of IL-rich and salt-rich phases with increasing feed solute concentrations.

Physical Properties at 20 ℃	Feed 18 wt%		Feed 20 wt%		Feed 22 wt%	
	K_3PO_4	C_4mimCl	K_3PO_4	C_4mimCl	K_3PO_4	C_4mimCl
μ [mPa.s]	5.6 ± 0.2	3.9 ± 0.1	9.9 ± 0.2	6.1 ± 0.2	15.1 ± 0.3	7.1 ± 0.2
σ (mN/m)	56 ± 2	48 ± 3	55 ± 2	50 ± 2	54 ± 2	52 ± 3
γ (mN/m)	0.4 ± 0.02		1.2 ± 0.03		2.3 ± 0.02	

Table 3
Bond numbers calculated for different channel diameters and ABS feed weight percentages.

	Channel internal diameter (mm)		
	0.20	**0.50**	**0.80**
18	0.36	2.27	5.81
20	0.14	0.86	2.20
22	0.08	0.50	1.28

phase has a slightly smaller contact angle (97 ± 2) than the salt phase (103 ± 2), meaning that it wets the channel wall more. The difference, however, is small and in dispersed patterns it may be possible to determine the continuous phase from the way the two phases are introduced in the channel. For consistency, in all experiments here, the ionic liquid is introduced first in the channel and acts as the continuous phase, followed by the salt rich phase.

5.1. Flow pattern maps

The flow patterns formed in the 0.5 mm channel are shown in Fig. 8 for the 22 feed wt% in a map with the mixture velocity and the IL rich phase volume fraction as coordinates. The lines in Fig. 8 show the boundaries of plug flow for different feed concentrations (18, 20 and 22 wt%). For the construction of the maps, the flow was considered plug when the dispersed phase drops would fill the entire channel diameter and have almost constant length (±3%) (see Fig. 7d).

Plug flow

In this regime, the ionic liquid phase is the continuous one and separates the convex shaped plugs of the salt phase, which are on average larger than the channel diameter as shown in Fig. 7d. Plug flow occupies a large area in the middle of the map in Fig. 8. The overall volume of the plugs is affected by the flow rates of the dispersed and continuous phases, while their formation is influenced by a combination of different factors including viscosity, interfacial tension, phase ratio and channel geometry. Two plug formation mechanisms were observed, squeezing and jetting (See Fig. 9). In the squeezing regime, the emerging dispersed phase blocks the channel inlet; pressure builds up in the continuous phase behind it which pushes the plug downstream the main channel until it detaches (see Fig. 9 a) (Garstecki et al., 2006). In the jetting regime, the dispersed phase forms a neck downstream the inlet (See Figs. 9 b and 10) which eventually breaks as a result of a Rayleigh instability (Utada et al., 2008). Once the plugs are formed, the interfacial forces help to maintain their regular shape.

As the flow rates increase, inertial forces also increase, and disturbances begin to form on the plug surface. In the transition between plug and dispersed flow, small satellite drops form behind the main plugs, as shown in Fig. 7f (plug & train flow). Plug & train flow occurs when the meniscus at the tails of the forming plugs in the inlet breaks into smaller satellite drops that spread into the continuous phase (see Fig. 10 c). Compared to organic-aqueous two-phase systems, for ABS systems this pattern dominates a larger area of the map because of their lower interfacial tension values.

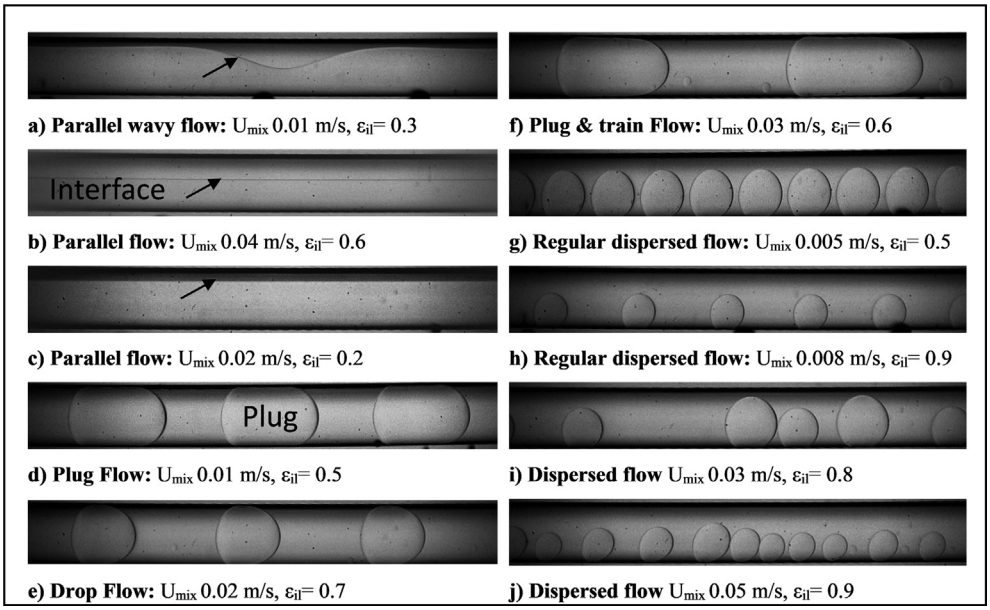

Fig. 7. Flow patterns observed in the 0.8 mm internal diameter channel with different mixture velocities (U_{mix}) and ionic liquid-rich phase volume fractions (ε_{IL}) for the 22 wt % ABS.

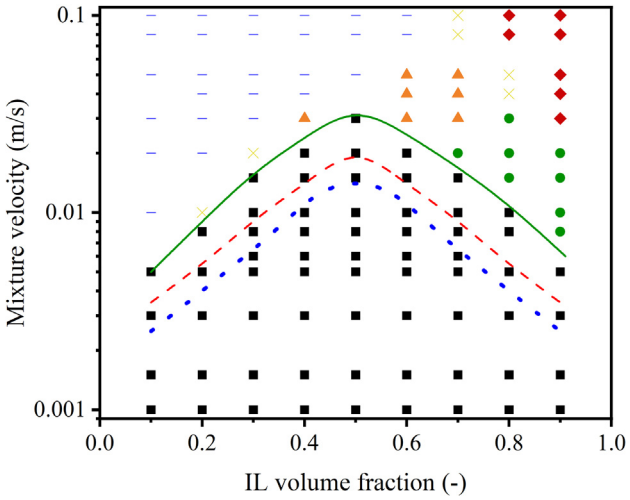

Fig. 8. Flow pattern map for 0.5 mm channel and ABS 22 feed wt%: (■) Plug flow; (-) Parallel flow; (♦) Dispersed flow; (●) Drop flow; (▲) Plug & train flow; (×) Intermittent flow; Plug flow boundary lines for 18,20 and 22 wt% ABS: (—) Boundary line 22 wt%;(---) Boundary line 20 wt%; (···) Boundary line 18 wt%.

When the viscous and inertia forces increase and become significantly larger than the interfacial tension forces, parallel flow is observed at low IL volume fractions.

Parallel flow

In parallel flow no break up occurs at the inlet, when the viscous and inertial forces dominate over the interfacial force. This flow pattern is dominated by gravity forces and occurs at high mixture velocities (see Fig. 8). The fluid with the lower density (ionic liquid phase) flows over the higher density fluid (salt phase) with a clear interface between the two (see Fig. 7 b). With organic solvent-aqueous two-phase mixtures annular flow is usually seen at high mixture velocities in small channels (Phakoukaki et al., 2022). In contrast, with the IL-ABS system, parallel flow is seen due to the large density difference between the ABS phases and their very similar contact angles with the channel wall.

Parallel wavy flow appeared close to the transition between parallel and plug flow at high mixture velocities and low ionic liquid volume fractions, ε_{IL} < 0.4 (See Fig. 7a). The shear force in the light fluid flowing over the high-density one caused ripples on the interface. With increasing velocities, small droplets of the two phases appear on the interface. In this case, the drag forces on the wavy interface overcome interfacial tension and gravity forces and lead to drop detachment (Al-Wahaibi and Angeli 2007). This pattern was only observed when the two phases were introduced in the channel at different velocities. Only parallel smooth flow was noticed at equal phase flowrates.

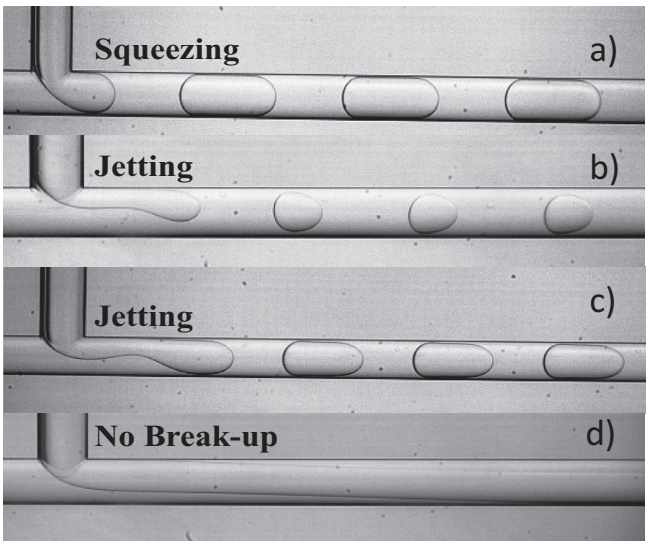

Fig. 9. Formation of different flow patterns at a *T*-Junction inlet configuration for the 0.5 mm channel diameter and 18 wt%. Ionic liquid (C_4mimCl) is the continuous phase and salt (K_3PO_4) is the dispersed.

Dispersed flow

The dispersed flow regime occurs at high mixture velocities and high ionic liquid volume fractions and occupies the top right side of the flow pattern map (See Fig. 8). As the mixture velocity increases the plugs decrease in length until their diameters become equal to the channel diameter (*drop flow*). With a further increase in the mixture velocity, drops smaller than the channel diameter form (See Fig. 7j). Due to the small interfacial tension values, drop break up is favoured at the *T*-Junction inlet, leading to small drops that do not fill the whole channel. With increasing channel diameter, the Bond number also increases (see Table 3), and gravity becomes important. As a result, the drops of the dispersed salt-rich phase for the 0.8 mm channel tend to settle to the bottom of the channel and may come in contact with the wall, because of the similar contact angles with the IL-rich phase (Fig. 7g). Moreover, smaller drops have been observed to travel faster than the larger drops due to the established flow profile in the channel, where velocity is higher in the centre and lower close to the channel wall. As the smaller drops travel faster downstream the channel, they encounter and coalesce with slightly larger drops ahead, resulting in the different sizes depicted in Fig. 7 i. At even higher mixture velocities the drops appear distorted to one side (See Fig. 7j). This is only seen in the 0.8 mm channel, where the salt-rich phase drops settle to the bottom of the channel because of the large Bond numbers (see Table 3). These drops experience lower velocity at their side in contact with the wall compared to that close to the centre of the channel, because of the velocity profile,which results in their deformation.

Intermittent

The intermittent flow regimes appear during the transitions between the main flow patterns, namely plug, parallel and dispersed flows. During intermittent flow, the flow patterns change over time along the main channel. For example, in the 0.5 mm internal diameter channel for volume fraction of the IL rich phase equal to 0.2 and 0.01 m/s mixture velocity, the pattern is intermittent (see Fig. 8) and changes between plug and parallel flow over time.

5.2. Effect of solute concentration and channel size on flow patterns

As it can be seen in Fig. 8, plug flow is present for all ionic liquid volume fractions at low mixture velocities. As the mixture velocity increases and at high ionic liquid volume fractions (ε_{IL} > 0.7) the plug flow transitions into regular drop flow, while at low ionic liquid volume fractions, parallel and parallel wavy flows are observed. The plug & train flow pattern appears at medium phase volume fractions and at high mixture velocities. As the mixture velocity is further increased U_{mix} > 0.07 m/s, parallel flow appears at a large part of the map for low and medium ionic liquid phase volume fractions, while at high fractions, dispersed flow of the salt-rich phase forms. By decreasing the inlet weight fractions of the ionic liquid and the salt from 22 to 18 wt% the plug flow region decreases (Fig. 8). The same flow patterns are observed with plug flow dominating at U_{mix} < 0.03 m/s for the 22 wt%, U_{mix} < 0.02-m/s for the 20 wt% and U_{mix} < 0.015 m/s for the 18 wt% ABS system.

The effect of channel diameter on the flow patterns and their transitions is seen in Fig. 11 for inlet weight fractions of 22 %.

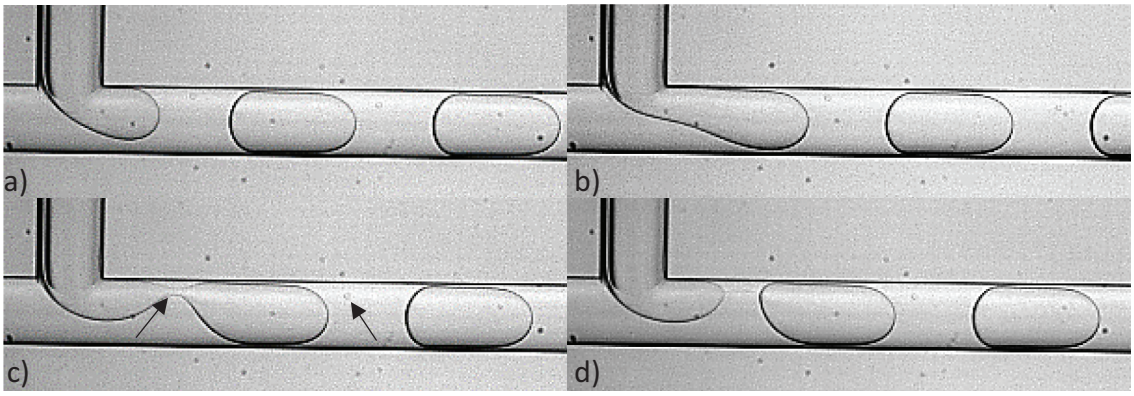

Fig. 10. Plug formation observed in the 0.5 mm channel at equal ionic liquid and salt phase volume fractions (ε_{IL}) for the 20 wt% ABS.

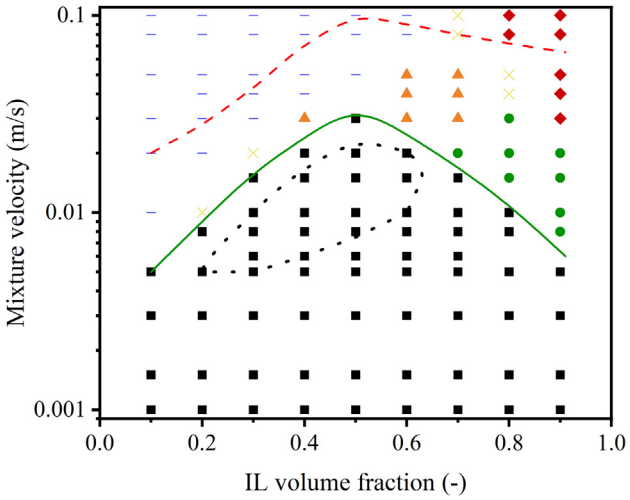

Fig. 11. Flow pattern map for 0.5 mm channel and ABS 22 feed wt%: (■) Plug flow; (-) Parallel flow; (♦) Dispersed flow; (●) Drop flow; (▲) Plug & Train flow; (×) Intermittent flow; Plug flow boundary lines for different channels: (---) Boundary line 0.2 mm; (—) Boundary line 0.5 mm; (···) Boundary line 0.8 mm.

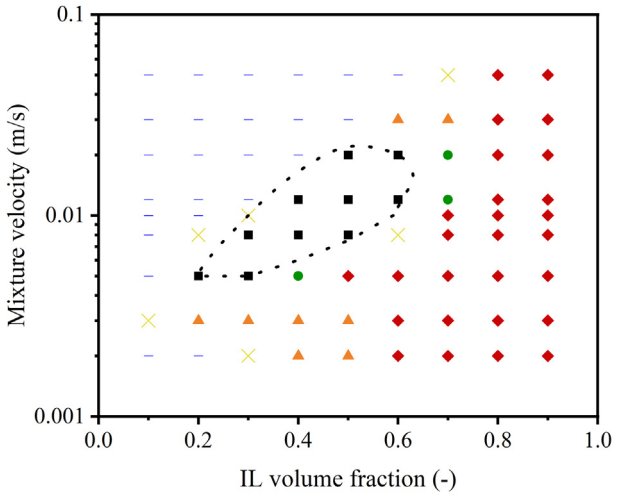

Fig. 12. Flow pattern map for 0.8 mm Internal diameter channel and ABS 22 feed wt %: (···) Boundary line 0.8 mm; (■)Plug flow; (-) Parallel flow; (♦) Dispersed flow; (●) Drop flow; (▲) Plug & Train flow; (×) Intermittent flow.

The plug flow transition lines are affected by the inertial and gravitational forces since interfacial tension forces do not change. In general, plug flow is limited to low mixture velocities compared to the literature, probably because of the low interfacial tension values of the ABS (Zhao and Middelberg, 2011).

As it can be seen, the area occupied by plug flow increases with decreasing channel diameter. The same trend was also observed for all three feed weight fractions (18, 20 and 22 wt%). At the 0.2 mm channel, the increased importance of interfacial forces compared to inertia and gravitational ones, allows plug flow to expand to high mixture velocities, compared to the other two channel diameters. For ionic liquid volume fractions $\varepsilon_{IL} > 0.5$ plug flow occurs at mixture velocities up to $U_{mix} = 0.08$ m/s.

For the 0.2 and 0.5 mm diameter channels the whole area below the transition lines shown in Fig. 11 is occupied by plug flow. However, in the 0.8 mm channel the area taken by plug flow is small and limited to the middle of the map; for mixture velocities $U_{mix} < 0.005$ m/s plug flow did not form at all (Fig. 12). At these low mixture velocities, dispersed phase formed at high ionic liquid volume fractions, plug & train flow at medium volume fractions and parallel flow at low volume fractions. The dispersed phase that formed below the plug flow boundary line was regular with drops of equal sizes as seen in Fig. 7g. This is probably due to the low interfacial tension values that cause drops to break at the inlet before filling the entire channel cross section. For the same channel configuration and similar mixture velocities and phase volume fractions, plug flow is reported in the literature with conventional organic-aqueous mixtures, instead of dispersed flow (Phakoukaki et al., 2022). The parallel flow seen at the low ionic liquid volume fractions and mixture velocities, probably forms because the two phases enter at very low velocities with no disturbances to break them to drops; in addition both phases have similar wettabilities with the channel wall and there is no preference for one of them to be the continuous phase.

6. Dimensionless flow pattern maps

As was shown in Figs. 8 and 11 the flow patterns of the ABS are affected by various parameters including, physical properties of the fluids and channel size. A generalized flow pattern map is required to predict the operating window of plug flow without resorting to experiments. A large number of studies have attempted to produce dimensionless flow pattern maps with a combination of dimensionless numbers as coordinates (Zhang et al., 2019; Yue et al., 2009; Yagodnitsyna et al., 2016; Kashid et al., 2010; Kashid and Agar, 2007; Yao et al., 2018). While the single dimensionless numbers proposed offer good predictions for specific experimental conditions, they are often limited by the number of forces they can accurately represent and as a result fail to predict flow patterns beyond the conditions under which they

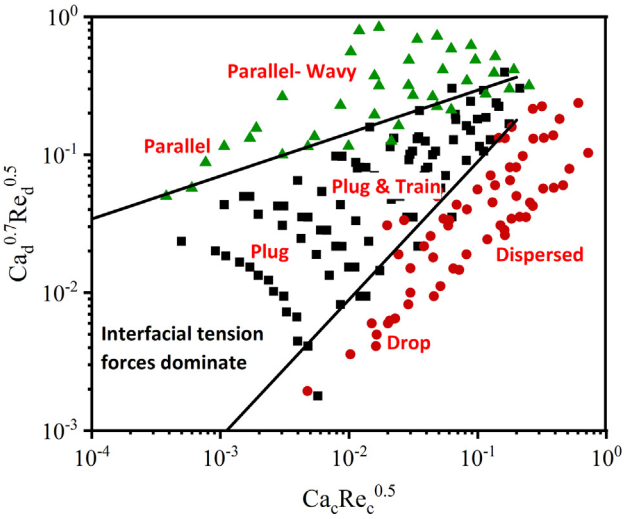

Fig. 13. Dimensionless flow pattern map: (■) Plug flow; (▲) Parallel flow; (●) Dispersed flow; (—) Plug flow boundary lines.

were obtained. Wu and Sundén (2019), combined Weber and Ohnesorge numbers to provide a dimensionless flow pattern map for low viscosity fluids. Similarly, Zhang et al. (2019), proposed a dimensionless flow pattern map by combining Reynolds and capillary numbers and showed the effects of the physical properties of the fluids; their proposed map showed good agreement with available literature data for both high and low viscosity fluids. To the authors' knowledge, there are no data on flow patterns and no maps in the literature for aqueous biphasic systems. The physical properties of the two phases of ABS significantly differ from those of the typical liquid–liquid systems, usually organic-aqueous, tested in microchannels. Inertial, viscous and interfacial forces are expected to dominate the flow compared to gravitational forces. Following this, flow pattern maps with coordinates $Ca_d^{0.7}$-$Re_d^{0.5}$ and $Ca_cRe_c^{0.5}$ as suggested by Zhang et al. (2019), are presented in Fig. 11 for mixture velocities ranging from 0.005 m/s to 0.1 m/s. The intermittent flow patterns observed were neglected. Ca_d and Re_d varied in the ranges 2.1×10^{-3}- 0.35 and 1.8×10^{-2} – 3.01, respectively. Ca_c and Re_c varied in the ranges $1.5\ x10^{-3}$ – 0.25 and $2.1\ x10^{-2}$ – 3.5, respectively.

The operational conditions where plug flow occurs are narrower that those suggested in the literature (Zhang et al., 2019). Based on the results, the following correlations in Eq. (5) and (6) are proposed for the boundaries of plug flow, for all three ABS solutions (18, 20 and 22 wt%) and channel diameters (0.2, 0.5 and 0.8 mm); the correlations were determined empirically.

$$Ca_d^{0.7}Re_d^{0.5} = 0.89(Ca_cRe_c^{0.5}) \quad (5)$$

$$Ca_d^{0.7}Re_d^{0.5} = 0.60\left(Ca_cRe_c^{0.5}\right)^{0.31} \quad (6)$$

Equations (5) and (6) represent the transition between plug and dispersed flow and between plug and parallel flow, respectively.

The lines separate the flow pattern map into 3 main areas, with different forces dominant in each. In the top right part of the map (Fig. 13) parallel flow prevails. In this region the dispersed phase inertial or viscous forces prevail over the interfacial ones. This is observed when the dispersed phase flow rate is larger than the continuous phase flow rate ($Q_d \gg Q_c$) or the dispersed phase viscosity (μ_d) is larger than the continuous phase one (μ_c). As can be seen from section 4 (Table 2) with increasing concentration of the solutes, the viscosity of the ionic liquid-rich phase increases compared to that of the salt-rich phase ($\mu_d \gg \mu_c$). At high flow rates strong interfacial disturbances occur and the pattern becomes parallel- wavy flow with small drops forming on the interface. In the centre of the map, plug flow is present and interfacial forces dominate over inertia and viscous ones. As the flow rates are increased at the top right of the plug flow area, irregular plug & train flow is present due to the effect of increasing inertia forces. In the bottom right-hand side of Fig. 13, the main patterns are dispersed and drop flow; in that region the continuous phase inertia or viscous forces dominate over the interfacial ones. This is observed for continuous phase flow rates greater than dispersed phase ones ($Q_d \ll Q_c$). Regular droplets that fill up the entire channel diameter (drop flow) form at low flow rates, and irregular ones (dispersed flow) form at high flow rates. It was also found that the plug flow region in the dimensionless map for IL-ABS is smaller than for conventional organic solvent -aqueous systems (Cubaud and Mason, 2008; Giri Nandagopal and Selvaraju, 2016; Bai et al., 2016; Kashid et al., 2007; Foroughi and Kawaji, 2011; Phakoukaki et al., 2022). This is attributed to the significantly smaller interfacial tension of the IL-ABS compared to the organic solvent-aqueous mixtures which favours small drops to form at low mixture velocities.

7. Conclusions

In this work an aqueous biphasic system (ABS) was formed composed of a hydrophilic ionic liquid, C_4mimCl, and a kosmotropic salt, K_3PO_4. A phase diagram was obtained and three different feed weight concentrations of the two solutes at equal %wt, and were used for further analysis, namely 18, 20 and 22 wt%. The properties of the two phases in the biphasic region for the selected feed concentrations were measured. It was found that with increasing weight concentration, the density of the salt-rich phase increased from 1.34 to 1.45 g/ml while that of the ionic liquid-rich phase slightly decreased from 1.09 to 1.07 g/ml. Moreover, by increasing the weight concentration of the two solutes, the interfacial tension significantly increased from 0.4 mN/m to 2.3 mN/m. As a result, with mixture volumes of 20 ml, the 18 wt% ABS mixture seperated completely after ~ 45 s, while the 22 wt% system separated in just 30 s (±4s). These separation times are shorter than in conventional polymer based ABS with interfacial tensions of approximately 0.1 mN/m.

The flow patterns formed with the ABS in the biphasic region were studied in small channels with different internal diameters (0.2, 0.5 and 0.8 mm). The main flow patterns observed included plug, drop, dispersed and parallel flow. The results revealed that the flow patterns observed were affected by the fluid physical properties and the channel size. Given the interfacial tension is low the conditions under which plug flow was observed was generally limited to low velocities. In the 0.2 mm ID channel plug flow occurred at all ionic liquid volume fraction for mixture velocities up to U_{mix} = 0.08 m/s. In the 0.5 and 0.8 mm ID channels the plug flow boundary significantly decreased. For the 0.8 mm channel plug flow was only observed at $0.005 < U_{mix} < 0.02$-m/. Furthermore, including all the measurements, a generalized flow pattern map was proposed with dimensionless coordinates $Ca_d^{0.7}Re_d^{0.5}$ and $Ca_cRe_c^{0.5}$, which shows the region of plug flow for all experimental conditions. The map may be used in the future to identify the plug flow regime without the need of further experimentation.

The results demonstrate that it is possible to change the properties of the ABS phases by varying the IL and salt concentrations and thus control the flow patterns that form in microfluidic devices. This ability to control droplet formation in an all-aqueous, surfactant-free and organic solvent-free system is extremely attractive for countless application of ABS in microchannels

including intensified processing, separations, analysis, drug delivery and synthesis.

Data availability

Data will be made available on request.

Acknowledgments

The authors would like to thank Johnson Matthey and the UK Engineering and Physical Sciences Research Council UK for the support via an iCASE studentship (EP/T517628/1).

References

Albertsson, Per-Åke, 1995. Aqueous biphasic systems. properties and applications in bioseparation. In: *Aqueous Biphasic Separations*, 21–30. Boston, MA: Springer US. https://doi.org/10.1007/978-1-4615-1953-9_2

Al-Wahaibi, T., Angeli, P., 2007. Transition between stratified and non-stratified horizontal oil-water flows. Part I: stability analysis. Chem. Eng. Sci. 62 (11), 2915–2928. https://doi.org/10.1016/j.ces.2007.01.024.

Angeli, P., Gavriilidis, A., 2008. Hydrodynamics of Taylor flow in small channels: a review. Proc. Inst. Mech. Eng., Part C: J. Mech. Eng. Sci. 222 (5), 737–751.

Assmann, N., Ładosz, A., Rudolf von Rohr, P., 2013. Continuous micro liquid-liquid extraction. Chem. Eng. Technol. 36 (6). https://doi.org/10.1002/ceat.201200557.

Bai, L., Zhao, S., Yuhang, F.u., Cheng, Y.i., 2016. Experimental study of mass transfer in water/ionic liquid microdroplet systems using micro-LIF technique. Chem. Eng. J. 298 (August), 281–290. https://doi.org/10.1016/j.cej.2016.04.034.

Bamberger, S., Brooks, D.E., Sharp, K.A., Van alstine, J.M., Webber, T.J., 1985. Preparation of Phase Systems and Measurement of Their Physicochemical Properties. In: Partitioning in Aqueous Two-Phase System. Elsevier, pp. 85–130. https://doi.org/10.1016/B978-0-12-733860-6.50010-4.

Berthod, A., Ruiz-Ángel, M.J., Carda-Broch, S., 2008. Ionic liquids in separation techniques. J. Chromatogr. A 1184 (1–2), 6–18. https://doi.org/10.1016/J.CHROMA.2007.11.109.

Cao, Z., Wu, Z., Sundén, B., 2018. Dimensionless analysis on liquid-liquid flow patterns and scaling law on slug hydrodynamics in cross-junction microchannels. Chem. Eng. J. 344, 604–615.

Ciceri, D., Perera, J.M., Stevens, G.W., 2014. The use of microfluidic devices in solvent extraction. J. Chem. Technol. Biotechnol. 89 (6), 771–786. https://doi.org/10.1002/jctb.4318.

Cubaud, T., Mason, T.G., 2008. Capillary threads and viscous droplets in square microchannels. Phys. Fluids 20, (5). https://doi.org/10.1063/1.2911716 053302.

Darekar, M., Singh, K.K., Mukhopadhyay, S., Shenoy, K.T., 2017. Liquid–liquid two-phase flow patterns in Y-junction microchannels. Ind. Eng. Chem. Res. 56 (42), 12215–12226. https://doi.org/10.1021/acs.iecr.7b03164.

Dore, V., Tsaoulidis, D., Angeli, P., 2012. Mixing patterns in water plugs during water/ionic liquid segmented flow in microchannels. Chem. Eng. Sci. 80, 334–341. https://doi.org/10.1016/j.ces.2012.06.030.

Dougherty, Ralph C., 2001. Density of Salt Solutions: Effect of Ions on the Apparent Density of Water. https://doi.org/10.1021/jp010097r.

Espitia-Saloma, E., Vázquez-Villegas, P., Aguilar, O., Rito-Palomares, M., 2014. Continuous aqueous two-phase systems devices for the recovery of biological products. Food Bioprod. Process. 92 (2), 101–112. https://doi.org/10.1016/j.fbp.2013.05.006.

Fang, Y.u., Frampton, J.P., Raghavan, S., Sabahi-Kaviani, R., Luker, G., Deng, C.X., Takayama, S., 2012. Rapid generation of multiplexed cell cocultures using acoustic droplet ejection followed by aqueous two-phase exclusion patterning. Tissue Eng. Part C: Methods 18 (9), 647–657. https://doi.org/10.1089/ten.tec.2011.0709.

Foroughi, H., Kawaji, M., 2011. Viscous oil-water flows in a microchannel initially saturated with oil: flow patterns and pressure drop characteristics. Int. J. Multiph. Flow 37 (9), 1147–1155. https://doi.org/10.1016/J.IJMULTIPHASEFLOW.2011.06.004.

Frampton, J.P., Lai, D., Sriram, H., Takayama, S., 2011. Precisely targeted delivery of cells and biomolecules within microchannels using aqueous two-phase systems. Biomed. Microdevices 13 (6), 1043–1051. https://doi.org/10.1007/s10544-011-9574-y.

Freire, Mara G., ed. 2016. *Ionic-Liquid-Based Aqueous Biphasic Systems*. Green Chemistry and Sustainable Technology. Berlin, Heidelberg: Springer Berlin Heidelberg. https://doi.org/10.1007/978-3-662-52875-4.

Garstecki, P., Fuerstman, M.J., Stone, H.A., Whitesides, G.M., 2006. Formation of droplets and bubbles in a microfluidic T-junction—scaling and mechanism of break-up. Lab Chip 6 (3), 437. https://doi.org/10.1039/b510841a.

Ghasemian, E., Najafi, M., Rafati, A.A., Felegari, Z., 2010. Effect of electrolytes on surface tension and surface adsorption of 1-hexyl-3-methylimidazolium chloride ionic liquid in aqueous solution. J. Chem. Thermodyn. 42 (8), 962–996. https://doi.org/10.1016/j.jct.2010.03.007.

Giri Nandagopal, M.S., Selvaraju, N., 2016. Prediction of liquid-liquid flow patterns in a Y-junction circular microchannel using advanced neural network techniques. Ind. Eng. Chem. Res. 55 (43), 11346–11362. https://doi.org/10.1021/acs.iecr.6b02438.

Görgényi, M., Dewulf, J.o., van Langenhove, H., Héberger, K., 2006. Aqueous salting-out effect of inorganic cations and anions on non-electrolytes. Chemosphere 65 (5), 802–810. https://doi.org/10.1016/j.chemosphere.2006.03.029.

Iqbal, M., Tao, Y., Xie, S., Zhu, Y., Chen, D., Wang, X.u., Huang, L., Peng, D., Sattar, A., Shabbir, M.A.B., Hussain, H.I., Ahmed, S., Yuan, Z., 2016. Aqueous two-phase system (ATPS): An overview and advances in its applications. Biological Procedures Online 18 (1). https://doi.org/10.1186/s12575-016-0048-8.

Jovanović, J., Zhou, W., Rebrov, E.V., Nijhuis, T.A., Hessel, V., Schouten, J.C., 2011. Liquid–liquid slug flow: hydrodynamics and pressure drop. Chem. Eng. Sci. 66 (1), 42–54. https://doi.org/10.1016/j.ces.2010.09.040.

Kashid, M.N., Agar, D.W., 2007. Hydrodynamics of liquid-liquid slug flow capillary microreactor: flow regimes, slug size and pressure drop. Chem. Eng. J. 131 (1–3), 1–13. https://doi.org/10.1016/J.CEJ.2006.11.020.

Kashid, M.N., Harshe, Y.M., Agar, D.W., 2007. Liquid−liquid slug flow in a capillary: an alternative to suspended drop or film contactors. Ind. Eng. Chem. Res. 46 (25). https://doi.org/10.1021/ie070077x.

Kashid, M.N., Gupta, A., Renken, A., Kiwi-Minsker, L., 2010. Numbering-up and mass transfer studies of liquid-liquid two-phase microstructured reactors. Chem. Eng. J. 158 (2), 233–240. https://doi.org/10.1016/J.CEJ.2010.01.020.

Long, F.A., McDevit, W.F., 1952. Activity coefficients of nonelectrolyte solutes in aqueous salt solutions. Chem. Rev. 51 (1), 119–169. https://doi.org/10.1021/cr60158a004.

Louros, C.L.S., Ana, F.M., Cláudio, C.M.S.S., Neves, M.G., Freire, I.M., Marrucho, J.P., Coutinho, J.A.P., 2010. Extraction of biomolecules using phosphonium-based ionic liquids + K3PO4 aqueous biphasic systems. Int. J. Mol. Sci. 11 (4), 1777–1791. https://doi.org/10.3390/ijms11041777.

Mastiani, M., Seo, S., Jimenez, S.M., Petrozzi, N., Kim, M.M., 2017. Flow regime mapping of aqueous two-phase system droplets in flow-focusing geometries. Colloids Surf., A 531 (October), 111–120. https://doi.org/10.1016/J.COLSURFA.2017.07.083.

McQueen, Lisa, Lai, David, 2019. Ionic liquid aqueous two-phase systems from a pharmaceutical perspective. Front. Chem. 7 (March). https://doi.org/10.3389/fchem.2019.00135.

Meagher, R.J., Light, Y.K., Singh, A.K., 2008. Rapid, continuous purification of proteins in a microfluidic device using genetically-engineered partition tags. Lab Chip 8 (4), 527. https://doi.org/10.1039/b716462a.

Neves, C.M.S.S., Ventura, S.P.M., Freire, M.G., Marrucho, I.M., Coutinho, J.A.P., 2009. Evaluation of cation influence on the formation and extraction capability of ionic-liquid-based aqueous biphasic systems. J. Phys. Chem. B 113 (15), 5194–5199. https://doi.org/10.1021/jp900293v.

Phakoukaki, Y.-V., O'Shaughnessy, P., Angeli, P., 2022. intensified liquid-liquid extraction of biomolecules using ionic liquids in small channels. Sep. Purif. Technol. 282, (February). https://doi.org/10.1016/j.seppur.2021.120063 120063.

Qian, J.-Y., Li, X.-J., Zan, W.u., Jin, Z.-J., Sunden, B., 2019. A comprehensive review on liquid-liquid two-phase flow in microchannel: flow pattern and mass transfer. Microfluid. Nanofluid. 23 (10). https://doi.org/10.1007/s10404-019-2280-4.

Quental, M.V., Passos, H., Kurnia, K.A., Coutinho, J.A.P., Freire, M.G., 2015. Aqueous biphasic systems composed of ionic liquids and acetate-based salts: phase diagrams, densities, and viscosities. J. Chem. Eng. Data 60 (6), 1674–1682.

Sattari-Najafabadi, M., Nasr Esfahany, M., Wu, Z., Sunden, B., 2018. Mass transfer between phases in microchannels: A review. Chem. Eng. Process. - Process Intensification 127, 213–237. https://doi.org/10.1016/j.cep.2018.03.012.

Sauret, A., Spandagos, C., Shum, H.C., 2012. Fluctuation-induced dynamics of multiphase liquid jets with ultra-low interfacial tension. Lab Chip 12 (18), 3380. https://doi.org/10.1039/c2lc40524e.

Seemann, R., Brinkmann, M., Pfohl, T., Herminghaus, S., 2012. Droplet based microfluidics. Rep. Prog. Phys. 75 (1), 016601.

Silva, D.F.C., Azevedo, A.M., Fernandes, P., Chu, V., Conde, J.P., Aires-Barros, M.R., 2012. Design of a microfluidic platform for monoclonal antibody extraction using an aqueous two-phase system. J. Chromatogr. A 1249 (August), 1–7. https://doi.org/10.1016/J.CHROMA.2012.05.089.

Singh, S.K., Savoy, A.W., 2020. Ionic liquids synthesis and applications: An overview. J. Mol. Liq. 297, 112038. https://doi.org/10.1016/j.molliq.2019.112038.

Smirnova, S.V., Ilin, D.V., Pletnev, I.V., 2021. Extraction and ICP-OES determination of heavy metals using tetrabutylammonium bromide aqueous biphasic system and oleophilic collector. Talanta 221, 121485.

Soohoo, J.R., Walker, G.M., 2009. Microfluidic aqueous two phase system for leukocyte concentration from whole blood. Biomed. Microdevices 11, 323–339. https://doi.org/10.1007/s10544-008-9238-8.

Teixeira, A.G., Agarwal, R., Ko, K.R., Grant-Burt, J., Leung, B.M., Frampton, J.P., 2018. Emerging biotechnology applications of aqueous two-phase systems. Adv. Healthcare Mater. 7 (6), 1701036. https://doi.org/10.1002/adhm.201701036.

Tsaoulidis, Dimitrios, Dore, Valentina, Angeli, Panagiota, Plechkova, Natalia v, Seddon, Kenneth R., 2013. Flow patterns and pressure drop of ionic liquid-water two-phase flows in microchannels. Int. J. Multiphase Flow 54 (September): 1–10. https://doi.org/10.1016/j.ijmultiphaseflow.2013.02.002.

Tsukamoto, M., Taira, S.u., Yamamura, S., Morita, Y., Nagatani, N., Takamura, Y., Tamiya, E., 2009. Cell separation by an aqueous two-phase system in a microfluidic device. The Analyst 134 (10), 1994. https://doi.org/10.1039/b909597g.

Utada, A.S., Fernandez-Nieves, A., Gordillo, J.M., Weitz, D.A., 2008. Absolute instability of a liquid jet in a coflowing stream. Phys. Rev. Lett. 100, (1). https://doi.org/10.1103/PhysRevLett.100.014502 014502.

Ventura, S.P.M., Neves, C.M.S.S., Freire, M.G., Marrucho, I.M., Oliveira, J., Coutinho, J. A.P., 2009. Evaluation of anion influence on the formation and extraction capacity of ionic-liquid-based aqueous biphasic systems. J. Phys. Chem. B 113 (27), 9304–9310. https://doi.org/10.1021/jp903286d.

Ventura, S.P.M., Sousa, S.G., Serafim, L.S., Lima, Á.S., Freire, M.G., Coutinho, J.A.P., 2011. Ionic liquid based aqueous biphasic systems with controlled PH: The ionic liquid cation effect. J. Chem. Eng. Data 56 (11), 4253–4260. https://doi.org/10.1021/je200714h.

Ventura, S.P.M., e Silva, F.A., Quental, M.V., Mondal, D., Freire, M.G., Coutinho, J.A.P., 2017. Ionic-liquid-mediated extraction and separation processes for bioactive compounds: past, present, and future trends. Chem. Rev. 117 (10), 6984–7052. https://doi.org/10.1021/acs.chemrev.6b00550.

Wang, C., Lei, Y.D., Wania, F., 2016. Effect of sodium sulfate, ammonium chloride, ammonium nitrate, and salt mixtures on aqueous phase partitioning of organic compounds. Environ. Sci. Technol. 50 (23), 12742–21279. https://doi.org/10.1021/acs.est.6b03525.

Wang, K., Luo, G., 2017. Microflow extraction: A review of recent development. Chem. Eng. Sci. 169, 18–33. https://doi.org/10.1016/j.ces.2016.10.025.

Weissenborn, Peter K., Pugh, Robert J., 1996. Surface Tension of Aqueous Solutions of Electrolytes: Relationship with Ion Hydration, Oxygen Solubility, and Bubble Coalescence. Journal of Colloid and Interface Science 184 (2), 550–563. https://doi.org/10.1006/JCIS.1996.0651.

Wu, Z., Sundén, B., 2019. Liquid-liquid two-phase flow patterns in ultra-shallow straight and serpentine microchannels. Heat and Mass Transfer/Waerme- Und Stoffuebertragung 55 (4), 1095–1108. https://doi.org/10.1007/s00231-018-2494-0.

Wu, B.o., Zhang, Y.M., Wang, H.P., 2008. Aqueous biphasic systems of hydrophilic ionic liquids + sucrose for separation. J. Chem. Eng. Data 53 (4), 983–995. https://doi.org/10.1021/je700729p.

Xu, C., Xie, T., 2017. Review of microfluidic liquid-liquid extractors. Ind. Eng. Chem. Res. 56 (27), 7593–7622. https://doi.org/10.1021/acs.iecr.7b01712.

Yagodnitsyna, Anna A., Kovalev, Alexander v., Bilsky, Artur v., 2016. Flow patterns of immiscible liquid-liquid flow in a rectangular microchannel with T-junction. Chem. Eng. J. 303 (November): 547–54. https://doi.org/10.1016/J.CEJ.2016.06.023.

Yang, Z., 2009. Hofmeister effects: an explanation for the impact of ionic liquids on biocatalysis. J. Biotechnol. 144 (1), 12–22. https://doi.org/10.1016/j.jbiotec.2009.04.011.

Yao, C., Zhao, Y., Chen, G., 2018. Multiphase processes with ionic liquids in microreactors: hydrodynamics, mass transfer and applications. Chem. Eng. Sci. 189 (November), 340–359. https://doi.org/10.1016/J.CES.2018.06.007.

Yue, J., Luo, L., Gonthier, Y., Chen, G., Yuan, Q., 2009. An experimental study of air-water taylor flow and mass transfer inside square microchannels. Chem. Eng. Sci. 64 (16), 3697–3708. https://doi.org/10.1016/J.CES.2009.05.026.

Zhang, Q.i., Liu, H., Zhao, S., Yao, C., Chen, G., 2019. Hydrodynamics and mass transfer characteristics of liquid-liquid slug flow in microchannels: the effects of temperature, fluid properties and channel size. Chem. Eng. J. 358 (February), 794–805. https://doi.org/10.1016/J.CEJ.2018.10.056.

Zhao, C.-X., Middelberg, A.P.J., 2011. Two-phase microfluidic flows. Chem. Eng. Sci. 66 (7), 1394–1411. https://doi.org/10.1016/j.ces.2010.08.038.

Ziemecka, I., van Steijn, V., Koper, G.J.M., Rosso, M., Brizard, A.M., van Esch, J.H., Kreutzer, M.T., 2011. Monodisperse hydrogel microspheres by forced droplet formation in aqueous two-phase systems. Lab Chip 11 (4), 620–664. https://doi.org/10.1039/C0LC00375A.